AIP | The Journal of Chemical Physics

Dynamical (e, 2e) studies using tetrahydrofuran as a DNA analog

C. J. Colyer, S. M. Bellm, B. Lohmann, G. F. Hanne, O. Al-Hagan et al.

Citation: J. Chem. Phys. **133**, 124302 (2010); doi: 10.1063/1.3491030
View online: http://dx.doi.org/10.1063/1.3491030
View Table of Contents: http://jcp.aip.org/resource/1/JCPSA6/v133/i12
Published by the American Institute of Physics.

Dynamical (e, 2e) studies using tetrahydrofuran as a DNA analog

C. J. Colyer,[1] S. M. Bellm,[1] B. Lohmann,[1,a)] G. F. Hanne,[2] O. Al-Hagan,[3] D. H. Madison,[3] and C. G. Ning[4]
[1]*ARC Centre of Excellence for Antimatter-Matter Studies, The University of Adelaide, Adelaide, South Australia 5005, Australia*
[2]*Physikalisches Institut, Universität Münster, Wilhelm-Klemm-Straße 10, 48149 Münster, Germany*
[3]*Department of Physics, Missouri University of Science and Technology, Rolla, Missouri 65409, USA*
[4]*Department of Physics and Key Laboratory of Atomic and Molecular NanoSciences of MOE, Tsinghua University, Beijing 100084, People's Republic of China*

(Received 26 July 2010; accepted 31 August 2010; published online 22 September 2010)

Triple differential cross sections for the electron-impact ionization of the outer valence orbital of tetrahydrofuran have been measured using the (e, 2e) technique. The measurements have been performed with coplanar asymmetric kinematics, at an incident electron energy of 250 eV and at an ejected electron energy of 10 eV, over a range of momentum transfers. The experimental results are compared with theoretical calculations carried out using the molecular three-body distorted wave model. The results obtained are important for gaining an understanding of electron driven processes at a molecular level and for modeling energy deposition in living tissue. © *2010 American Institute of Physics*. [doi:10.1063/1.3491030]

I. INTRODUCTION

There is considerable interest in the ionization dynamics of molecules for the interactions of ionizing radiation with biological matter. In the past decade, experimental studies have indicated that secondary particles produced by the primary ionizing event can play a significant role in radiation damage to DNA.[1] In the ionization process, large numbers of secondary electrons with comparatively low energies (0–20 eV) are liberated, which then interact with biomolecules such as sugars,[2,3] water,[4] and the DNA and RNA bases.[5–7] Precisely defining the nature of these electron-biomolecule interactions presents a number of experimental and theoretical challenges.[8] One approach to characterizing them is to probe isolated molecules in the gas phase. In the studies of radiation damage in DNA, this approach of studying the processes occurring in the constituent units, such as the isolated bases, sugar, and phosphate units, has been proven to be a valuable one and has enabled an understanding of some of the highly complex molecular dynamics that are occurring.[9] The primary focus of the present study is to further understand electron-molecule interactions using smaller biomolecules to compare directly with the components of larger biological systems.

Here, we examine the electron-impact ionization of tetrahydrofuran (THF) C_4H_8O using the electron-electron coincidence technique or (e, 2e) technique. This is a powerful method for obtaining detailed information on the electron-impact-induced ionization dynamics of atoms and molecules.[10] In the (e, 2e) technique, a projectile electron with well-defined energy and momentum ionizes an atomic or a molecular target. The scattered projectile and the ejected target electron are detected in time coincidence and their energies and momenta are determined. The method can also be used to elucidate the bound electron structure of a target, which is known as electron momentum spectroscopy (EMS).[11] While many EMS studies have been performed on both atomic and molecular targets, only a few experimental (e, 2e) measurements have been undertaken to investigate the dynamics of molecular ionization, and these have been mostly limited to diatomic and small polyatomic molecules including H_2,[12–14] N_2,[15–19] H_2O,[20,21] CO_2,[19,22] C_2H_2,[23] N_2O,[24] and most recently CHOOH.[25] This has been largely due to the experimental and theoretical challenges involved in molecular studies including, on the theory side, the description of a multicentered target, and on the experimental side, the difficulties in resolving different molecular states that are often closely spaced. Madison and Al-Hagan[26] reviewed the recent theoretical work that has been performed for some of these molecules.

Here, we report on the first dynamical (e, 2e) study of THF, a larger polyatomic molecule of chemical and biological importance. It can be regarded as a structural unit in a number of biological molecules including the sugar moiety in the sugar-phosphate backbone of DNA and RNA, as illustrated in Fig. 1. This backbone structure can be represented as a series of THF molecules bonded to phosphate units and DNA bases. The current study extends our previous (e, 2e) investigations on the ionization dynamics of the H_2O (Ref. 20) and formic acid biomolecules.[25]

While no previous dynamical (e, 2e) studies of THF have been reported in literature, it has been investigated by EMS to study ring puckering and torsion in the ring.[27,28] A THF molecule is a five membered heterocyclic ring compound that undergoes pseudorotation. This is an internal motion that involves of out-of-plane ring puckering vibrations that occur in a way that makes the phase of the puckering rotate about the ring.[29] Three possible conformations of THF

a)Author to whom correspondence should be addressed. Electronic mail: birgit.lohmann@adelaide.edu.au.

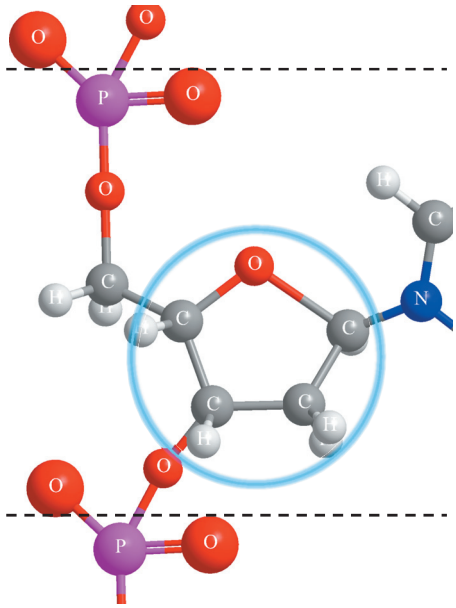

FIG. 1. The segment of the sugar-phosphate backbone of a single strand of DNA with an attached cytosine molecule. The location of THF in the strand is highlighted by the blue ring. The repeating unit of the strand is marked by the black dashed lines.

are produced by pseudorotation in the gas phase. These are of C_1, C_2, and C_s point group symmetry. All three conformations are very close in energy; indeed, calculations predict that the energy differences are within the error of many computational models.[27] There has been some debate and there is still no general consensus about which conformation is the lowest energy and most populated conformer.[27,30] However, experimental evidence indicates that both C_2 and C_s conformers coexist at room temperature. Yang *et al.*[27] compared the simulated orbital momentum density probability distributions for the two conformers to distributions measured using EMS and determined that the C_s structure is the preferred conformer and the lowest energy structure. A second study undertaken by the same group at higher energy found that at room temperature, around 55% of THF molecules are in the C_s conformation and 45% in the C_2 form.[28] Guiliani *et al.*[30] determined, from high-resolution photoabsorption spectroscopy supported by high-level *ab initio* calculations, that both conformers exist at 298 K, with a Boltzmann analysis predicting 44.5% of THF molecules are in the C_s form and 55.5% in the C_2 form. Recently, Dampc *et al.*[31] also observed evidence of both conformers in photoelectron spectroscopy (PES) studies.

Both elastic and inelastic electron scattering cross sections are of considerable interest for use in the studies of charged particle track structure analysis, which is an approach used to simulate radiation damage in biological systems. The damage induced by a single source of radiation is modeled by following the track of a primary particle and all secondary charged particles that are produced in ionizing collisions. As an example, recently, Champion[32] developed a Monte Carlo code to simulate electron transport and energy deposition in biological material. Isolated water spheres were considered to simulate processes in biological media. To accurately model the chemistry, detailed information is required on the initial spatial distribution of events involving both ionization and excitation along the charged particles' path. Differential cross sections are an important source of this information as they enable a complete three dimensional description of the deposition of energy as a function of angle. The knowledge of these cross sections for both the initial primary particle and the secondary charged particles that are produced in ionizing collisions is therefore required. The data produced by experimentally measuring selected key cross sections provide an important means of testing the theoretical calculations that are used to derive the extensive cross section data needed to model these processes. A more detailed description of radiation damage in biological systems may be gained by using charged particle track structure techniques that include cross sections for other significant biomolecules such as THF.[33] It is anticipated that the results presented here will be relevant for this purpose.

II. EXPERIMENTAL APPARATUS

The direct single ionization of a ground state target particle A by electron impact can be described by[34]

$$e^-(E_0,\mathbf{k}_0) + \mathrm{A} \rightarrow \mathrm{A}^+ + e^-(E_a,\mathbf{k}_a) + e^-(E_b,\mathbf{k}_b), \tag{1}$$

where A^+ is the ionized particle, and E_0, E_a, E_b and $\mathbf{k}_0$, $\mathbf{k}_a$, $\mathbf{k}_b$ are the kinetic energies and momenta of the incident, scattered, and ejected electrons, respectively. Energy and momentum conservation requires

$$E_0 = E_a + E_b + \varepsilon_i, \tag{2}$$

$$\mathbf{q} = \mathbf{k}_0 - \mathbf{k}_a - \mathbf{k}_b, \tag{3}$$

where ε_i is the ionization potential of an electronic orbital in the target species and $\mathbf{q}$ is the ion recoil momentum. The recoil energy of the ion is small compared to the energy of the other particles and is thus neglected. The momentum difference between the incident and the scattered electrons is given by the momentum transfer vector $\mathbf{K}$,

$$\mathbf{K} = \mathbf{k}_0 - \mathbf{k}_a. \tag{4}$$

The triple differential cross section (TDCS), represented by

$$\frac{d^5\sigma}{d\Omega_a d\Omega_b dE_a}, \tag{5}$$

is a measure of the probability that after ionization of a target species by a projectile with energy E_0 and momentum $\mathbf{k}_0$, two electrons will be produced with energies E_a and E_b and momenta $\mathbf{k}_a$ and $\mathbf{k}_b$ into the solid angles Ω_a and Ω_b. Due to the large number of kinematic parameters associated with the ionization process, there exist different geometric variations of the TDCS, which probe different physical properties of the process. In this study, we shall refer only to the coplanar asymmetric geometry, which implies that all the electrons are detected in-plane, that the scattered and ejected electron energies are vastly different, and finally that the scattered electron detection angle θ_a is fixed. Figure 2 shows the reaction kinematics in the present study.

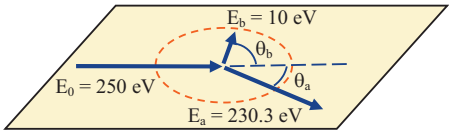

FIG. 2. The reaction kinematics in coplanar asymmetric geometry. Ionization is induced by a beam of 250 eV incident electrons. The ejected target electrons with energies of 10 eV are detected to the left of the projectile beam and the scattered projectile electrons to the right.

This study has been conducted in a conventional (e, 2e) spectrometer, which has been well documented in literature,[24] and so will only be briefly described here. The spectrometer is housed in a large vacuum chamber that is constructed from nonmagnetic 310 stainless steel, with an internal mu-metal lining to reduce penetrating external magnetic fields. At the interaction region, magnetic fields are further reduced to less than 1 mG by three orthogonal pairs of Helmholtz coils.

An incident beam of electrons is produced from a thoriated tungsten filament and extracted via a Pierce grid element. The resulting electrons are transported into the interaction region via a five-element cylindrical electrostatic lens system. The resultant electron beam has an energy resolution of approximately 0.5 eV full width at half maximum (FWHM) and a diameter of approximately 1 mm at the interaction region.

The tetrahydrofuran vapor target enters the interaction region via a 0.69 mm internal diameter stainless steel capillary. The vapor is obtained from a liquid sample, of 99.9% stated purity (Sigma-Aldrich, Australia), which is held in a glass vial, with any trapped gases expelled via several freeze-pump-thaw cycles. To prevent condensation, the beam-forming capillary and associated gas handling system is held at approximately 75 °C, while the vacuum chamber is heated to approximately 50 °C. To help avoid deposition of THF on the vacuum chamber and electron optics, a cold finger is mounted approximately 5 cm above the interaction region to collect the target beam. Made from 310 stainless steel with an oxygen free, high thermal conductivity copper disk at the collection end, the cold finger is filled externally with liquid nitrogen.

Electrons exiting the interaction region are detected via two hemispherical electron energy analyzers, mounted on independently rotatable turntables concentric with the interaction region. Each of the hemispherical energy analyzers is preceded by a five-element electrostatic lens system. After passing through the hemisphere, the electrons are detected by a channel electron multiplier (Sjuts).

The angular cross sections are determined from the measured signal by rotating the ejected electron energy analyzer around the detection plane and by measuring signal at each scattering angle for a set period of time. Electron binding energy spectra can also be measured by fixing the two electron energy analyzers at a given pair of angles. The scattered electron energy is then treated as the independent variable and the coincidence signal is measured at each scattered electron energy for a set period of time.

The energies of the hemispherical electron energy analyzers and the electron gun have been calibrated using the $L_{2,3}MM$ Auger spectrum of argon,[35] while the angular calibration of the analyzers has been determined using the well-defined minimum in the differential cross section for elastic scattering of 60 eV electrons from argon.[36] To ensure that the apparatus was operating correctly throughout the measurements, consistency checks were performed regularly. This involved measuring the TDCS for He(1s) ionization under similar kinematics and confirming that it remained in good agreement with distorted wave Born approximation (DWBA) calculations.

III. THEORY

The details of the molecular three-body distorted wave (M3DW) approach have been presented in a previous publication.[26] In short, the THF molecular wave function was calculated using density functional theory along with the standard hybrid B3LYP (Ref. 37) functional by means of the ADF 2007 (Amsterdam density functional) program[38] with the TZ2P (triple-zeta with two polarization functions) Slater-type basis sets. The experimental cross sections represent an average over all molecular orientations and the previous M3DW calculations have approximated this average using the orientation averaged molecular orbital (OAMO). The OAMO approximation works very well for highly symmetric molecular states. However, the OAMO is zero for the 9b and 12a′ states of THF due to antisymmetric cancellations of different regions of space. To avoid these cancellations, we have averaged the absolute value of the wave function instead of the actual wave function. The three continuum distorted waves are calculated using spherically symmetric radial potentials obtained for either the neutral molecule or the ion. The potentials are a sum of a static part, the exchange potential of Furness and McCarthy,[39] and the correlation-polarization potential of Perdew and Zunger.[40] The static part contains the interaction of a continuum electron with the bound molecular electrons plus the nuclei. The electronic part is obtained by finding the interaction potential for a continuum electron with the molecular charge density (either neutral or ion) and averaging this interaction over all orientations. For the nuclear part, the charge of each nucleus is placed on a thin spherical shell centered on the molecular center-of-mass. Finally, the final state electron-electron interaction [normally called postcollision interaction (PCI)] is included directly in the final state wave function, which means that PCI is included in all orders of perturbation theory.

IV. RESULTS AND DISCUSSION

Figure 3 shows the coincidence binding energy spectrum for the outer valence region of tetrahydrofuran. The incident and ejected electron energies were fixed at 250 and 10 eV, respectively, while the scattered electron energy was scanned across a range of energies. The detection angles for the scattered and ejected electrons were chosen to be −10° and 90°, respectively. The experimental (e, 2e) coincidence energy resolution was determined to be 1.5 eV FWHM, from the width of the helium 1s binding energy peak measured under the same kinematics. This has been used to define the peak width, to fit a sum of Gaussian functions to the peaks in the

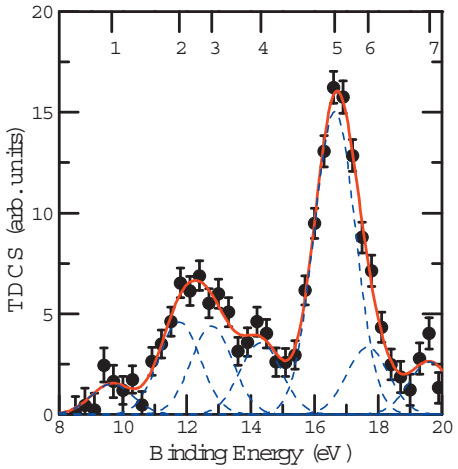

FIG. 3. The measured binding energy spectrum for the outer valence region of tetrahydrofuran, fitted with a sum of Gaussian functions using the coincidence energy resolution as the peak width.

spectrum shown in Fig. 3. We have used seven Gaussian functions to fit the data, as labeled 1–7 in Fig. 3.

The outer valence region of THF is complicated by the presence of many molecular orbitals; indeed, there are eleven molecular orbitals for each of the C_2 and C_s conformers of THF that are calculated to lie within the binding energy range we have measured. The highest occupied molecular orbitals (HOMOs) of THF are dominated by the O(2p) and H(1s) orbitals.[41] Table I shows the binding energy for each orbital, as well as the assignments and energies as determined via EMS (Ref. 28) and PES.[41] Our resolution of 1.5 eV is insufficient to resolve contributions from the two major conformers. Photoelectron spectroscopy measurements of Giuliani *et al.*[30] with a significantly higher resolution of 50 meV also found the two conformers indistinguishable, although they were able to observe vibrational structure associated with the excitation of the ground ionic state in these measurements. The first peak in Fig. 3 at an energy of 9.7 eV is fitted by a single Gaussian function and assigned to the combined outermost valence orbitals of THF (9b+12a′), which correspond to the outermost orbital of the C_2 and C_s conformers, respectively. This first peak is not completely resolved from the next broad peak in the experimental data, which we have fitted with two Gaussian functions, and includes contributions from up to eight orbitals, four attributed to each conformer. The largest peak at approximately 16.8 eV is also fitted by two Gaussian functions and is assigned as a combination of four different orbitals. These are 7a+8a′ at 16.6 eV and 5b+7a′ at 17.7 eV.

Here, we present triple differential cross sections for the ionization of the combined outermost valence orbitals (9b +12a′), corresponding to the outermost orbitals of the C_2 and C_s conformers. The experiments were performed at a relatively low incident electron energy of 250 eV, while the ejected electron energy was chosen to be 10 eV. The examination of the momentum density probability distributions for the HOMO presented in Ning *et al.*[28] indicates that for recoil ion momenta below 0.5 a.u., one may expect the contribution from the 12a′ orbital to be considerably larger than that of the 9b orbital. Specifically, under the chosen kinematics, this translates into ejected electron angles around 60°, where the 12a′ state dominates, and angles around 120°, where the contributions are thought to be approximately equal.

Figures 4(a)–4(c) show the present experimental results for the HOMO of tetrahydrofuran. The relatively large error bars on the experimental data result from the small magnitude of the coincidence cross section. Traditionally, the angular distributions are divided into two regions: the binary region ranging from 0° to 180° and the recoil region that ranges from 180° to 360°. The binary region is aptly named because the structure here is attributed to single binary collisions. Depending on the kinematics, the TDCS in the binary region may contain strong signatures of the orbital structure.[42] In contrast, the recoil structure arises from pro-

TABLE I. Tetrahydrofuran binding energies (in eV), with the error in the Gaussian peak position quoted in brackets. Giuliani *et al.* (Ref. 30) did not report energies and orbital assignments for the peak designated number 7; instead, assignment and energies are reported by Yang *et al.* (Ref. 27).

		Theory[a]			
	Present results	C_2	C_s	EMS[b]	PES[c]
1	9.7 (0.6)	9.94 (9b)	9.91 (12a′)	9.7	9.67
2	11.8 (0.6)	11.65 (11a)	11.65 (11a′)	12.14	11.41
		12.20 (10a)	11.89 (8a″)		11.99
3	12.8 (0.6)	12.43 (8b)	12.26 (10′)		12.48
		12.62 (9a)	12.30 (7a″)		12.90
4	14.3 (0.6)	14.21 (7b)	13.74 (6a″)	14.54	14.00
		14.82 (6b)	14.49 (9a′)		14.45
		14.95 (8a)	15.29 (5a″)		15.29
5	16.6 (0.6)	16.57 (7a)	16.29 (8a′)	16.74	16.70
6	17.7 (0.6)	16.93 (5b)	16.83 (7a′)		
7	19.6 (0.6)	18.64 (6a)[d]	18.67 (6a′)[d]	19.74	19.42

[a]Reference 30.
[b]Reference 28.
[c]Reference 41.
[d]Reference 27.

cesses whereby the ejected electron produced by an initial binary collision undergoes subsequent recoil scattering from the target nucleus.

As the experimental data are not on an absolute scale, their maximum values have been normalized to unity. In Fig. 4(a), it is evident from the relative size of the peaks in the binary and recoil regions that there is a large amount of interaction between the ejected electron and the target nucleus under this kinematic arrangement. The data have been fitted with a function of the form

$$f(\theta_b) = \sum_n a_n P_n(\cos(\theta_b - \alpha)), \tag{6}$$

where P_n are the Legendre polynomials. The binary and recoil regions have been fitted separately. The fit is to enable better visualization of the distributions and no physical meaning is attributed to the function. The same approach has been used previously by Avaldi *et al.*[43] and Cavanagh and Lohmann.[24] Table II shows the value of the symmetry angles for the binary and recoil regions determined from the fit, α_{bin} and α_{rec}, respectively, the highest-order Legendre polynomial used in each fit n_{max}, and the direction of the momentum transfer.

The data in Fig. 4(a) for a scattering angle of −5° exhibit a local minimum very close to the momentum transfer direction in both binary and recoil lobes. Although the Legendre polynomial fit does not follow the clear dip in the experimental data, the symmetry angle from the fit α_{bin} (see Table II) coincides almost exactly with the momentum transfer direction θ_K.

At a scattering angle of −10°, the data in Fig. 4(b) exhibit a broader binary peak, again with a local minimum near the momentum transfer direction. This minimum appears deeper than in Fig. 4(a). The ratio of binary intensity to recoil intensity is much higher than for the −5° scattering angle. The kinematics at the −10° scattering angle is close to bound Bethe ridge conditions. On the bound Bethe ridge, the kinematics satisfies the condition that all momentum is transferred to the bound, stationary target electron during the collision. Under such conditions, the collision kinematics corresponds to a binary e-e collision, where the ion plays no role, and practically no recoil lobe is expected.

For the largest scattering angle of −15°, the binary peak is again very broad. The relative size of the recoil peak is also small. This appears similar to the findings from our previous study on formic acid, where the size of the recoil peak relative to the binary peak decreased greatly as the scattering angle was increased and was significantly smaller than for water under the same kinematics. It was suggested previously[25] that this trend is due to the location of the molecules' center-of-mass, which, in the cases of both formic acid and tetrahydrofuran, is quite some distance from a charge center. Drawing on the arguments presented in Ref. 44, it is postulated that the lack of nuclear charge at the center-of-mass results in a decreased recoil scattering.

It is harder to discern a clear minimum in the experimental binary peak for this case, but the symmetry angle determined from the Legendre polynomial fit is close to the momentum transfer direction. In Figs. 4(a) and 4(b), the

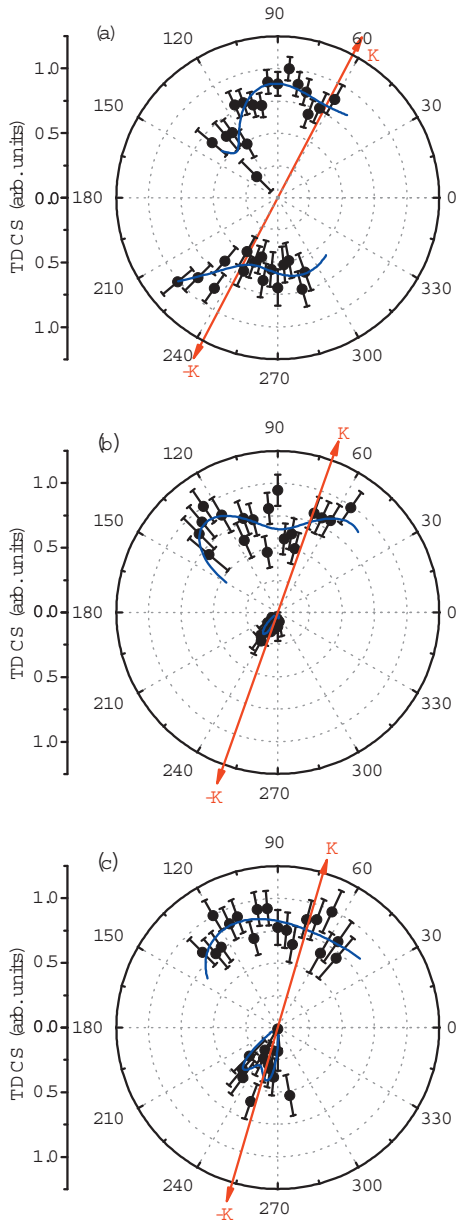

FIG. 4. Polar plot of the triple differential cross sections for ionization of the combined 9b+12a′ valence orbital of tetrahydrofuran, with E_0=250 eV and E_b=10 eV. The scattered electron detection angles and the corresponding momentum transfers are (a) −5°, |K|=0.40 a.u.; (b) −10°, |K|=0.75 a.u.; and (c) −15°, |K|=1.11 a.u. The points are the experimental data and the solid line is a fit of Eq. (6) to the data. The positions of the momentum transfer vectors, **K** and **−K**, are indicated by the arrows.

symmetry angle determined from the fits is close to the minima observed in the experimental data. This suggests that the THF cross sections might have a double lobe structure in the binary region, symmetric close to the momentum transfer direction. As the momentum transfer is increased when the scattered electron angle is increased, the kinematic conditions for scattering angles of −5°, −10°, and −15° correspond to being below, on, and above the bound Bethe ridge; the double lobe structure appears below the bound Bethe ridge, becomes more pronounced on the Bethe ridge, and then barely discernable above the bound Bethe ridge at −15°. Double binary peak structures have previously been observed for ionization of atomic p-states, so this may be a signature of the O(2p) contribution to the cross section.[45]

TABLE II. Values of the symmetry angles α_{bin} and α_{rec} for fits of Eq. (6) to the binary and recoil regions, respectively, of the experimental (e, 2e) cross section for the ionization of the combined outermost valence orbitals (9b+12a′) of tetrahydrofuran. n_{max} is the highest-order polynomial used for each fit. θ_K and θ_{-K} represent the direction of the momentum transfer vector **K** in each case.

θ_a (deg)	n_{max}	α_{bin} (deg)	θ_K (deg)	n_{max}	α_{rec} (deg)	θ_{-K} (deg)
−5	3	62.5	62.3	2	289.2	242.3
−10	2	88.5	70.5	3	236.2	250.5
−15	2	65.7	73.6	3	244.4	253.6

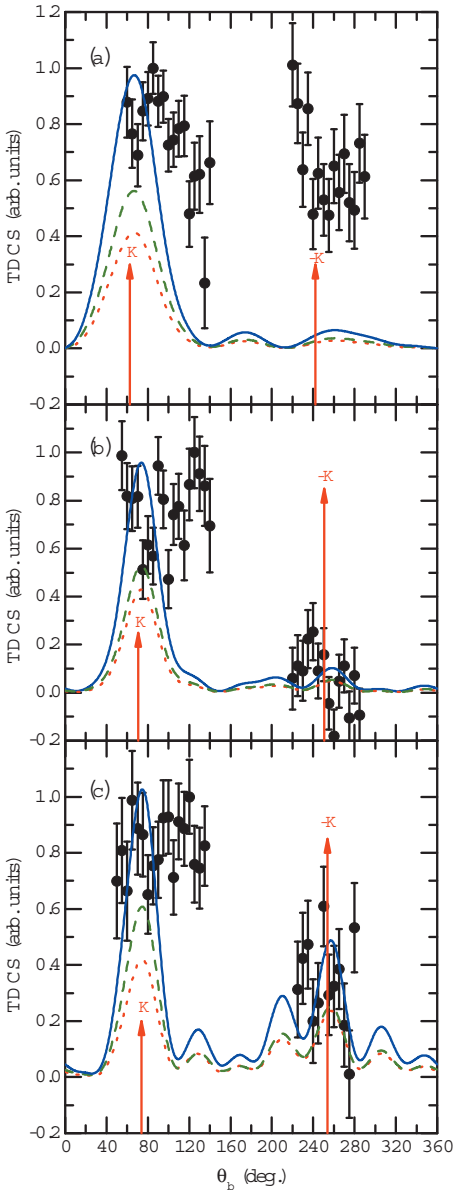

FIG. 5. Plot of the triple differential cross sections for ionization of the combined 9b+12a′ valence orbital of tetrahydrofuran, with E_0=250 eV and E_b=10 eV. The scattered electron detection angles and the corresponding momentum transfers are the same as in Fig. 4. Points are the experimental data. Dashed curve (green): M3DW calculation for the 12a′ orbital. Dotted curve (red): M3DW calculation for the 9b orbital. Solid curve (blue): M3DW calculation for the combined 9b+12a′ orbitals.

Figure 5 compares the present results with the M3DW theoretical calculations. It is seen that the M3DW predicts a binary peak very close to the momentum transfer direction for both the 9b and 12a′ states, which means that the sum has also a peak for this direction where the experiment finds a minimum. As mentioned above, atomic cross sections for p-states have been found to have a double binary peak with a minimum near the momentum transfer direction. Assuming that this split peak originates from the 2p nature of the molecular state, the M3DW would not be able to reproduce this feature of the data since the averaging process automatically produces an s-state type of angular dependence, which means that the cross sections will have a binary peak near the momentum transfer direction. PCI causes a slight shift of the binary peak to larger scattering angles, which is consistent with symmetry angles listed in Table II. However, the experimental shift is much larger for −10° and −15° than the M3DW predicts. As predicted by Ning *et al.*,[28] we find that the 12a′ state dominates the 9b state in the binary peak region near 60°, and above 120°, the two states make almost equivalent contributions.

The M3DW predicts recoil peaks in qualitative agreement with experiment for −10° and −15° but not −5°. Very recently, Toth and Nagy[46] reported a very similar DWBA calculation for ionization of CH_4. The M3DW reduces to the DWBA if PCI is neglected in the final state wave function. Toth and Nagy showed that the size of the recoil peak is related to the strength of the nuclear term in the static potential and they attributed underestimating the magnitude of the recoil peak to a nuclear interaction that is too weak, which is caused by the spreading of the nuclear charge over a spherical shell. Since the M3DW properly predicts the relative height of the recoil peak for the two larger angles that correspond to smaller impact parameter collisions, this "weakening" of the nuclear scattering is evidently more important for large impact parameters than small one. On the other hand, it is difficult to see why backscattering should be more important for large impact parameters than small one.

V. CONCLUSIONS

We present dynamical (e, 2e) studies for the THF molecule, which is a model compound to investigate electron interactions with the deoxyribose molecule. The measured binding energies and orbital assignments are in good agreement with the available EMS and PES data. The TDCSs at all scattered electron angles investigated show a broad binary peak. Similar to the formic acid monomer, experimental

cross sections for THF exhibit a significant change in the binary peak shape as the scattering angle is varied and a ratio between the recoil peak magnitude and the binary peak magnitude, which is much smaller than that observed for ionization of water under the same kinematics.

The M3DW was generally in qualitative agreement with the experimental data, except that the experimental data exhibited a split binary peak, while the theory only had a single peak and the theoretical recoil peak for the smallest scattering angle was much smaller than the experimental data. Also, the theoretical width of the binary peak was smaller than the experimental data, indicating a possible problem with the initial bound state momentum distribution. For the two larger scattering angles, the M3DW produced qualitative agreement with the recoil peak and reasonably good agreement with the ratio of binary to recoil peak heights. Considering the complexity of the molecule, we think that the M3DW was in surprisingly good agreement with the experimental data.

ACKNOWLEDGMENTS

This work was supported by the Australian Research Council Centre of Excellence for Antimatter-Matter Studies and the American NSF under Grant No. 0757749. C.G.N. would like to acknowledge the support of the National Natural Science Foundation of China under Contract No. 10704046. G.F.H. was supported by the Heinrich-Hertz-Stiftung des Landes Nordrhein-Westfalen, Germany, and an Australian International Science Linkages Programme grant. O.A.-H. would like to acknowledge the support of the Saudi Ministry of Higher Education's King Abdullah Bin Abdul-Aziz Scholarship. Moreover, C.J.C. would like to acknowledge the support of an Australian Postgraduate Award.

[1] B. Boudaïffa, P. Cloutier, D. Hunting, M. A. Huels, and L. Sanche, Science **287**, 1658 (2000).
[2] S. Ptasińska, S. Denifl, P. Scheier, and T. D. Mark, J. Chem. Phys. **120**, 8505 (2004).
[3] C. J. Colyer, V. Vizcaino, J. P. Sullivan, M. J. Brunger, and S. J. Buckman, New J. Phys. **9**, 41 (2007).
[4] A. Muñoz, F. Blanco, G. García, P. A. Thorn, M. J. Brunger, J. P. Sullivan, and S. J. Buckman, Int. J. Mass. Spectrom. **277**, 175 (2008).
[5] S. Denifl, S. Ptasinska, M. Cingel, S. Matejcik, P. Scheier, and T. D. Mark, Chem. Phys. Lett. **377**, 74 (2003).
[6] G. Hanel, B. Gstir, S. Denifl, P. Scheier, M. Probst, B. Farizon, M. Farizon, E. Illenberger, and T. D. Märk, Phys. Rev. Lett. **90**, 188104 (2003).
[7] M. A. Huels, I. Hahndorf, E. Illenberger, and L. Sanche, J. Chem. Phys. **108**, 1309 (1998).
[8] P. Możejko and L. Sanche, Radiat. Phys. Chem. **73**, 77 (2005).
[9] P. Swiderek, Angew. Chem., Int. Ed. **45**, 4056 (2006).
[10] A. Lahmam-Bennani, J. Phys. B **24**, 2401 (1991).
[11] I. E. McCarthy and E. Weigold, Rep. Prog. Phys. **51**, 299 (1988).
[12] M. Cherid, A. Lahmam-Bennani, A. Duguet, R. W. Zurales, R. R. Lucchese, M. C. Dal Cappello, and C. Dal Cappello, J. Phys. B **22**, 3483 (1989).
[13] D. S. Milne-Brownlie, M. Foster, J. Gao, B. Lohmann, and D. H. Madison, Phys. Rev. Lett. **96**, 233201 (2006).
[14] E. M. Staicu Casagrande, A. Naja, F. Mezdari, A. Lahmam-Bennani, P. Bolognesi, B. Joulakian, O. Chuluunbaatar, O. Al-Hagan, D. H. Madison, D. V. Fursa, and I. Bray, J. Phys. B **41**, 025204 (2008).
[15] J. P. Doering and J. Yang, Phys. Rev. A **60**, 2176 (1999).
[16] A. J. Murray, M. J. Hussey, J. Gao, and D. H. Madison, J. Phys. B **39**, 3945 (2006).
[17] A. Naja, E. M. Staicu-Casagrande, A. Lahmam-Bennani, M. Nekkab, F. Mezdari, B. Joulakian, O. Chuluunbaatar, and D. H. Madison, J. Phys. B **40**, 3775 (2007).
[18] L. R. Hargreaves, C. Colyer, M. A. Stevenson, B. Lohmann, O. Al-Hagan, D. H. Madison, and C. G. Ning, Phys. Rev. A **80**, 062704 (2009).
[19] A. Lahmam-Bennani, E. M. Staicu Casagrande, and A. Naja, J. Phys. B **42**, 235205 (2009).
[20] D. S. Milne-Brownlie, S. J. Cavanagh, B. Lohmann, C. Champion, P. A. Hervieux, and J. Hanssen, Phys. Rev. A **69**, 032701 (2004).
[21] C. Kaiser, D. Spieker, J. Gao, M. Hussey, A. Murray, and D. H. Madison, J. Phys. B **40**, 2563 (2007).
[22] M. J. Hussey and A. J. Murray, J. Phys. B **38**, 2965 (2005).
[23] L. Avaldi, R. Camilloni, and G. Stefani, Phys. Rev. A **41**, 134 (1990).
[24] S. J. Cavanagh and B. Lohmann, J. Phys. B **32**, L261 (1999).
[25] C. J. Colyer, M. A. Stevenson, O. Al-Hagan, D. H. Madison, C. G. Ning, and B. Lohmann, J. Phys. B **42**, 235207 (2009).
[26] D. H. Madison and O. Al-Hagan, J. Atomic Molecular Optical Phys. **2010**, 367180 (2010).
[27] T. Yang, G. Su, C. Ning, J. Deng, F. Wang, S. Zhang, X. Ren, and Y. Huang, J. Phys. Chem. A **111**, 4927 (2007).
[28] C. G. Ning, Y. R. Huang, S. F. Zhang, J. K. Deng, K. Liu, Z. H. Luo, and F. Wang, J. Phys. Chem. A **112**, 11078 (2008).
[29] D. O. Harris, G. G. Engerholm, C. A. Tolman, A. C. Luntz, R. A. Keller, H. Kim, and W. D. Gwinn, J. Chem. Phys. **50**, 2438 (1969).
[30] A. Giuliani, P. Limão-Vieira, D. Duflot, A. R. Milosavljevic, B. P. Marinkovic, S. V. Hoffmann, N. Mason, J. Delwiche, and M. J. Hubin-Franskin, Eur. Phys. J. D **51**, 97 (2009).
[31] M. Dampc, B. Mielewska, M. R. F. Siggel-King, G. C. King, and M. Zubek, Chem. Phys. **359**, 77 (2009).
[32] C. Champion, Phys. Med. Biol. **48**, 2147 (2003).
[33] M. Fuss, A. Muñoz, J. C. Oller, F. Blanco, D. Almeida, P. Limão-Vieira, T. P. D. Do, M. J. Brunger, and G. García, Phys. Rev. A **80**, 052709 (2009).
[34] E. Weigold and I. E. McCarthy, *Electron Momentum Spectroscopy* (Kluwer Academic, Plenum, 1999).
[35] L. O. Werme, T. Bergmark, and K. Siegbahn, Phys. Scr. **8**, 149 (1973).
[36] R. Panajotovic, D. Filipovic, B. Marinkovic, V. Pejcev, M. Kurepa, and L. Vuskovic, J. Phys. B **30**, 5877 (1997).
[37] C. Lee, W. Yang, and R. G. Parr, Phys. Rev. B **37**, 785 (1988).
[38] C. F. Guerra, J. G. Snijders, G. T. Velde, and E. J. Baerends, Theor. Chem. Acc. **99**, 391 (1998).
[39] J. B. Furness and I. E. McCarthy, J. Phys. B **6**, 2280 (1973).
[40] J. P. Perdew and A. Zunger, Phys. Rev. B **23**, 5048 (1981).
[41] M. Yamauchi, H. Yamakado, and K. Ohno, J. Phys. Chem. A **101**, 6184 (1997).
[42] H. Ehrhardt, K. Jung, G. Knoth, and P. Schlemmer, Z. Phys. D: At., Mol. Clusters **1**, 3 (1986).
[43] L. Avaldi, R. Camilloni, E. Fainelli, and G. Stefani, J. Phys. B **25**, 3551 (1992).
[44] O. Al-Hagan, C. Kaiser, D. Madison, and A. J. Murray, Nat. Phys. **5**, 59 (2009).
[45] A. Lahmam-Bennani, H. F. Wellenstein, A. Duguet, and M. Rouault, J. Phys. B **16**, 121 (1983).
[46] I. Tóth and L. Nagy, J. Phys. B **43**, 135204 (2010).